# Recombination Losses Above and Below the Transport Percolation Threshold in Bulk Heterojunction Organic Solar Cells

*Aren Yazmaciyan, Martin Stolterfoht, Paul L. Burn, Qianqian Lin, Paul Meredith,* and Ardalan Armin**

**Achieving the highest power conversion efficiencies in bulk heterojunction organic solar cells requires a morphology that delivers electron and hole percolation pathways for optimized transport, plus sufficient donor:acceptor contact area for near unity charge transfer state formation. This is a significant structural challenge, particularly in semiconducting polymer:fullerene systems. This balancing act in the model high efficiency PTB7:PC70BM blend is studied by tuning the donor:acceptor ratio, with a view to understanding the recombination loss mechanisms above and below the fullerene transport percolation threshold. The internal quantum efficiency is found to be strongly correlated to the slower carrier mobility in agreement with other recent studies. Furthermore, second-order recombination losses dominate the shape of the current density–voltage curve in efficient blend combinations, where the fullerene phase is percolated. However, below the charge transport percolation threshold, there is an electric-field dependence of first-order losses, which includes electric-field-dependent photogeneration. In the intermediate regime, the fill factor appears to be limited by both first- and second-order losses. These findings provide additional basic understanding of the interplay between the bulk heterojunction morphology and the order of recombination in organic solar cells. They also shed light on the limitations of widely used transport models below the percolation threshold.**

## 1. Introduction

The bulk heterojunction (BHJ) configuration is the dominant architecture in donor:acceptor organic solar cells. Power conversion efficiencies (PCEs) above 10% have been achieved with the most recent record approaching 13%.[1–4] In any solar cell, optimizing both charge photogeneration and charge extraction is a central challenge. This is achieved in BHJ devices by maximizing the donor:acceptor "molecular-scale" interfacial contact area, while simultaneously providing percolated transport pathways for the extraction of both electrons and holes at their respective electrodes without recombination.[5] This is a major challenge, particularly so in polymer:small molecule systems such as those containing the once ubiquitous fullerene-based acceptors.[6]

Independent of the material system, understanding the basic mechanisms behind charge generation and extraction, and indeed how they interact, is central to achieving PCEs closer to theoretical Shockley and Queisser limit.[7] In this

A. Yazmaciyan
School of Mathematics and Physics
The University of Queensland
Brisbane 4072, Australia

Dr. M. Stolterfoht
Institute of Physics and Astronomy
University of Potsdam
Karl-Liebknecht-Str. 24-25, D-14476 Potsdam-Golm, Germany

Prof. P. L. Burn, Prof. P. Meredith
Centre for Organic Photonics and Electronics (COPE)
School of Mathematics and Physics and School of Chemistry and Molecular Biosciences
The University of Queensland
Brisbane 4072, Australia
E-mail: paul.meredith@swansea.ac.uk

Dr. Q. Lin
School of Physics and Technology
Wuhan University
Wuhan, Hubei Province 430072, P. R. China

Prof. P. Meredith, Dr. A. Armin
Department of Physics
Swansea University
Singleton Park
Swansea SA2 8PP, Wales, UK

Dr. A. Armin
Centre for Engineered Quantum Systems (EQuS)
School of Mathematics and Physics
The University of Queensland
Brisbane 4072, Australia
E-mail: ardalan.armin@swansea.ac.uk

The ORCID identification number(s) for the author(s) of this article can be found under https://doi.org/10.1002/aenm.201703339.

**DOI: 10.1002/aenm.201703339**

 

regard, considerable effort has been directed toward studying exciton dissociation and the role of the intermediate charge transfer (CT) state—the efficient separation of which is a necessary condition for photogeneration of free charge carriers in semiconductors which are excitonic at room temperature.[8–11] Furthermore, it is increasingly recognized that minimizing free carrier recombination is also a prerequisite for high PCEs, and this is now a subject of growing and significant interest.[11–13]

Historically, Onsager theory based on the work of Langevin for the diffusive recombination of ions in a plasma has been used to understand the recombination physics of free carriers in organic solar cells.[14,15] The theory predicts that both bimolecular recombination (second-order recombination between non-geminate electrons and holes), and the dissociation rate of CT states are dependent on the sum of the electron and hole mobilities. In systems where the mobilities are imbalanced, this approximates to the faster carrier mobility. Following these basic models, the field-assisted separation of CT states in low dielectric constant materials was presented by Braun,[16] and is considered to be a more realistic interpretation of Onsager's theory.[14] Adaptations to the Braun model to account for the complex energy potential landscape in BHJs arising from the non-uniformly mixed donor:acceptor phases have also been developed and provide a more sophisticated and realistic framework for CT state dissociation.[17,18] In addition, it has recently been shown that charge photogeneration correlates well with the slower carrier mobility rather than the faster species,[19] and there are likely to be transport regimes that are dependent upon the range and ratio of the mobilities.[20–23] Other related explanations put forward for understanding the CT state dissociation include the impact of the active layer morphology in the form of delay time between exciton dissociation and bimolecular recombination;[24] an entropic driving force that is dependent on the number of available free carrier sites for a CT state dissociation event;[8] the role of singlet exciton and high CT state energies (conventionally referred to as the "hot" CT states);[25] and energetic disorder.[26] In these models, and the associated measurements, an electric-field dependence of charge generation (as predicted by Braun) has not been thoroughly studied or observed in high efficiency donor:acceptor systems, although it does appear in nonoptimized, lower efficiency combinations.[13] The role of the slower carrier and electric-field dependence of photogeneration thus remain outstanding questions in our search for "the perfect morphological balance." Recent studies provide evidence for the presence of field-dependent first-order losses and charge generation in BHJ organic solar cells.[27]

Motivated by these considerations, we have undertaken a study whereby the slower carrier mobility was systematically varied in the model high efficiency BHJ blend, poly({4,8-bis[(2-ethylhexyl)oxy]benzo[1,2-b:4,5-b′]dithiophene-2,6-diyl}{3-fluoro-2-[(2-ethylhexyl)carbonyl]thieno[3,4-*b*]thiophenediyl}):[6,6]-phenyl-$C_{71}$-butyric acid methyl ester (PTB7:$PC_{71}BM$). This was achieved by controlling the donor:acceptor blend ratio and engineering regimes, where the fullerene component was above and below its physical percolation threshold required for efficient electron transport. We then studied the internal quantum efficiency (IQE) as a function of light intensity as well as first- and second-order recombination losses as a function of applied electric field. We observed a strong correlation between the IQE, acceptor percolation, and the slower carrier mobility, plus the involvement of both first- and second-order losses depending upon the blend regime. In the limiting case below the fullerene percolation threshold, we find evidence of field-assisted charge photogeneration as predicted by Braun, but it is questionable whether these blends are actually true BHJs.

## 2. Material System

While there are many different combinations of donor and acceptor that could have been utilized in this study, PTB7:$PC_{71}BM$ blends were chosen as they have been shown to deliver high PCEs with relatively well-controlled and understood structure–property relationships. For example, Hedley et al. investigated the morphology of PTB7:$PC_{71}BM$ blends, and showed how the high boiling point solvent additive 1,8-diiodooctane (DIO) modifies the nanostructure of the photoactive layer using photocurrent mapping.[5] This work reinforced the importance of the BHJ morphology and how it affects the device performance metrics. Foertig et al. reported the geminate and non-geminate recombination losses in PTB7:$PC_{71}BM$ solar cells using a combination of transient and carrier extraction measurement techniques such as transient photovoltage, time-delayed collection field, and voltage-dependent charge extraction.[28] They observed field-dependent charge generation in PTB7:$PC_{71}BM$ devices processed without DIO, and attributed it to poor polaron pair dissociation. Kniepert et al. also investigated the effect of solvent additive on charge generation, extraction, and recombination in PTB7:$PC_{71}BM$ solar cells.[29] Their experimental device characteristics and numerical simulations showed the complexity of modeling the current density–voltage (*J*–*V*) curves and the importance of the interplay between carrier mobility, recombination, and field-dependent generation for explaining the measured *J*–*V* characteristics. Hence, given the abundance of comparative data, the PTB7:$PC_{71}BM$ blend was chosen for our study.

## 3. Results

### 3.1. Carrier Mobilities

**Figure 1**a shows a plot of the faster and slower carrier mobilities for solar cells containing PTB7:$PC_{71}BM$ blends ranging from 40% to 95% polymer content (w/w) measured using the Resistance-dependent PhotoVoltage (RPV) technique.[30] It is important to note that the devices all had similar junction thicknesses (≈100 nm) to avoid performance and transport differences arising from electro-optical effects, and were prepared without an additive in the processing solvent. The advantage of using RPV is that it enables accurate measurement of both the slower and faster carrier mobilities when they are different in device structures and under conditions that are operationally representative of organic solar cells. For blends containing up to ≈65 wt% of PTB7, the slower and faster carriers have approximately the same mobilities (we term this the plateau region), and it is not possible to assign the mobilities to a particular carrier type. Reducing the fullerene content leads to the mobility of the slower carrier decreasing exponentially. This is consistent with

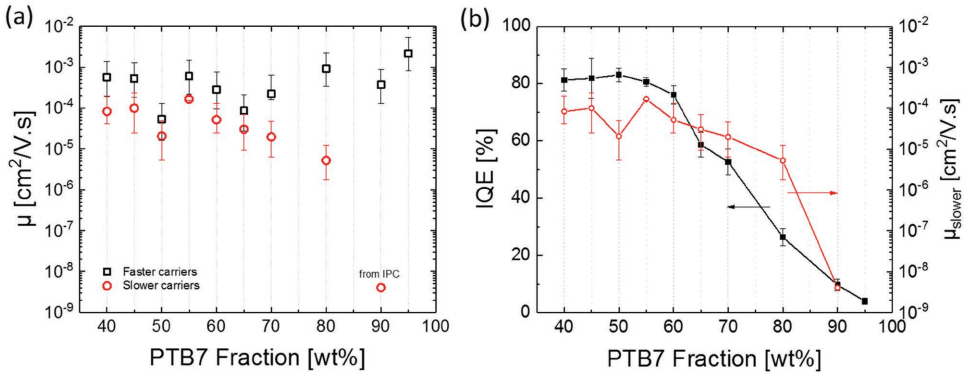


**Figure 1.** a) Slower and faster carrier mobilities for PTB7:$PC_{71}BM$ solar cells with ≈100 nm thick junctions obtained by RPV under operationally representative conditions. Error bars were estimated from the uncertainties in both the measured junction thicknesses and the carrier transit times (see the Experimental Section). b) IQE versus PTB7 Fraction (and slower carrier mobility) for the same devices in (a). Error bars represent the standard deviation from the mean value of the IQEs calculated in the visible part of the spectrum (see Figure S1, Supporting Information).

the electron being the slower carrier in devices with >65 wt% of PTB7 as the fullerene becomes diluted. The error bars in the carrier mobility values arise from the uncertainty in measuring the junction thickness and in identifying the carrier transit times.[31]

### 3.2. Internal Quantum Efficiency

In Figure 1b, we present the corresponding IQEs of the devices presented in Figure 1a. These IQEs were carefully determined by taking into account the parasitic absorptions and cavity effects in a procedure involving transfer matrix analysis, accurate knowledge of the optical constants of the components in the device stack, near normal incidence reflectance measurements, and determination of the external quantum efficiency (EQE).[32] There is a clear correspondence between the slower carrier mobility and the IQE, and we also note that the IQE under 1 sun illumination (as per this experimental regime) is the product of the charge generation and extraction efficiencies. At low incident light intensities, the IQE is dominated by the charge generation efficiency since bimolecular recombination is essentially negligible. We will return to this point when determining the IQE as a function of light intensity.

### 3.3. Current–Voltage (*J–V*) Characteristics

Device metrics such as short-circuit current density ($J_{SC}$), Fill Factor (FF), and PCE as a function of PTB7 content in the blend are shown in **Figure 2** (average of five measurements). Consistent with the IQEs shown in Figure 1, each of the three performance parameters maps onto the slower carrier mobility. Although these solar cells were not designed to deliver the optimized highest PCE possible for PTB7:$PC_{71}BM$ as reported by He et al.,[33] our hero device performance was comparable to those reported in the literature.[5,34] We achieved this by using a chlorobenzene (CB) and 1,2-dichlorobenzene (DCB) mixture as the processing solvent, and without DIO. The processing conditions used in this study gave an optimum blend ratio of 1:1 (PTB7:$PC_{71}BM$) by weight, which is slightly different to the generally reported 1:1.5 by weight blend with different processing solvent combinations.[5,29,35]

### 3.4. Light-Intensity-dependent Photocurrent and IQE

Light-Intensity-dependent photocurrent (IPC) measurements enable identification and quantification of both first- and second-order recombination losses within operational solar cells and photodetectors.[31,36–39] Photocurrents were measured at an illuminant wavelength of 532 nm as a function of the light intensity from ≈$10^{-6}$ to 1 W $cm^{-2}$ for all blend ratios, and representative raw IPC plots are shown in Figure S3 in the Supporting Information. The slope of the linear fit to the photogenerated current density–light intensity plot on a log–log scale provides significant insight in regard to bimolecular recombination losses. Deviation from a slope $\alpha = 1$ is evidence for the existence of bimolecular recombination. For example,

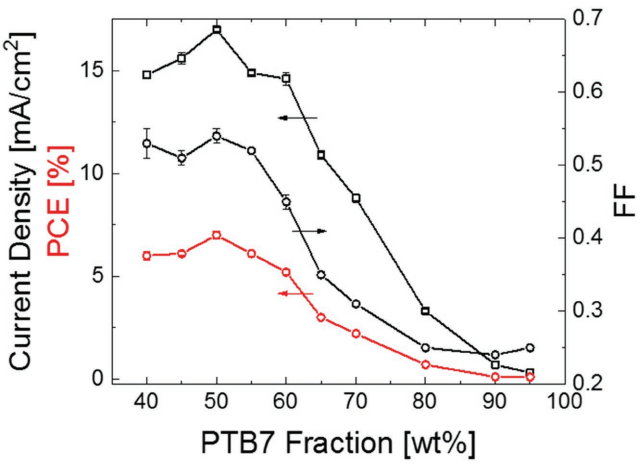


**Figure 2.** Current density (black, open squares), FF (black, open circles), and PCE (red, open circles) of devices with PTB7 content ranging from 40% to 95% by weight. The error bars are the standard deviations obtained from the measurements of five different cells and the values are the mean averages (see Figure S2 in the Supporting Information for $V_{OC}$ versus PTB7 content plot).

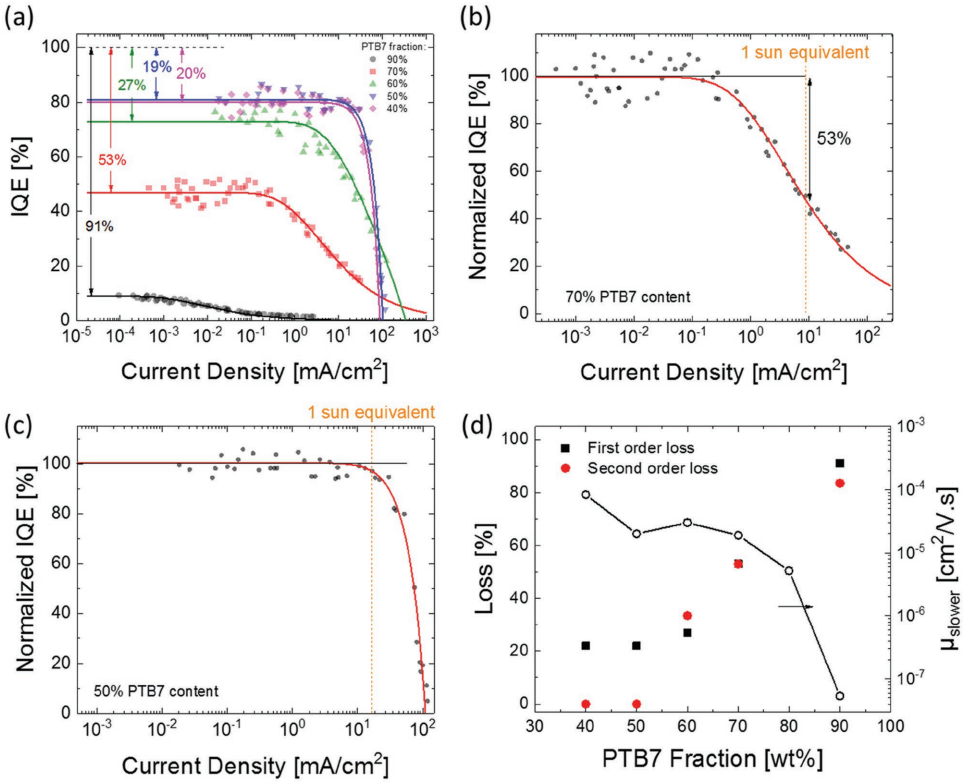


**Figure 3.** a) First-order recombination losses for several PTB7:$PC_{71}BM$ blends calculated from IQE versus short-circuit current density ($J_{SC}$) plots. In b) and c), the second-order recombination losses occurring in 70% and 50% PTB7 fraction devices are shown, respectively, to exemplify how they can be determined from the normalized IQE versus short-circuit current density at 1 sun equivalent (see Figure S4 in the Supporting Information for other devices). It should be noted that the second-order losses shown in the normalized IQE–$J_{sc}$ plot were calculated based on exclusion of first-order recombination losses and take only surviving charge carriers into account. d) First- and second-order losses together with slower carrier mobility as a function of PTB7 fraction. The solid lines in (a)-(c) are fittings based on a modified Shockley model accounting for imperfect charge collection.[11]

a three-quarter power dependence of the photocurrent on the light intensity has been predicted and shown for nonlinear losses induced by the formation of slower carrier space charges in systems with imbalanced mobilities.[40,41] Thus, measuring the IPC response over a broad range of light intensities allows accurate determination of the deviation point from the linear to sublinear regimes and vice versa. The IPC results were replotted by taking the derivative of the photocurrent versus incident light power to more accurately identify and quantify both the geminate (first-order) and non-geminate (second-order) recombination losses as previously described.[31] As such, the raw IPC data were used to create the IQE versus current density plots in **Figure 3**a in order to focus on recombination losses related to charge generation and extraction processes. Furthermore, we plotted the IQE versus short-circuit current density, which enables a true comparison of the deviation in current densities of different devices. As shown in our previous studies, the current density at which the IQE deviates from the constant value is proportional to the slower carrier mobility, which becomes the bottleneck for efficient extraction of photogenerated carriers.[31,42] It is thus clear that accurate determination of the IQE as a function of incident light intensity is a prerequisite for the identification and quantification of recombination losses, and this will now be demonstrated in more detail.

### 3.5. Determination of First-Order Losses

From the IQE plots of Figure 3a, we can quantify the first-order losses for each of the blend ratios (shown as the arrows and corresponding percent values). The plateau in IQE at lower current densities corresponds to the linear regime observed in the photocurrent versus laser power plots (see Figure S3, Supporting Information), where first-order recombination is the only loss mechanism as described earlier. We do not qualify or quantify the exact first-order processes at play here, but trap-assisted free carrier recombination (Shockley–Read–Hall), geminate exciton, or CT state recombination/relaxation are typically evoked. Free carrier generation is the most efficient around the 1:1 blend ratio as one would expect, and falls off precipitously upon dilution of the fullerene consistent with all other measurements.

### 3.6. Determination of Second-Order Losses

To exemplify the determination of the second-order (bimolecular) recombination losses at 1 sun, the IQE (normalized to 100%) as a function of short-circuit current density for a device containing 70 wt% of PTB7 is shown in Figure 3b. The deviation of the normalized IQE from 100% at an intensity equivalent to the AM1.5G standard (8 mA $cm^{-2}$) indicates the fraction

of free carriers in the device that undergo second-order recombination under operational conditions. For comparison, in a 1:1 optimized blend (Figure 3c), the second-order loss is almost negligible at 1 sun and at short circuit.

Figure 3d summarizes first- and second-order losses for different blend compositions plotted versus the slower carrier mobilities. Both first- and second-order losses increase as the slower carrier mobility decreases, with a clear correlation between the data sets. At PTB7 fractions greater than 60%, fullerene physical percolation begins to break down. We note this is not a true percolation threshold given the heterogeneous nature of the morphology, i.e., it does not represent a classical thermodynamic phase transition. That said, as the slower carrier mobility decreases exponentially, the photocurrent losses increase concomitantly. In the next section, we examine these losses as a function of voltage in order to investigate their dependencies on electric field. Finally, we note that the solid lines in Figure 3a–c are not just empirical fits or guides to the eye, but are derived from fittings based on a modified Shockley model accounting for imperfect charge collection—this also is relevant for the field dependence analysis.[11]

### 3.7. Electric-Field Dependence of First- and Second-Order Losses

The *J*–*V* characteristics of devices with 50%, 70%, and 90% PTB7 content by weight are plotted in **Figure 4**. The blend ratios shown in Figure 4a–c were particularly selected to highlight the trends in the field dependence of the FF. The FF of a solar cell is conventionally considered as the manifestation of the field dependence of the photogenerated current which is given by the Shockley equation in most inorganic semiconductor solar cells.[7] For disordered semiconducting materials such as those utilized in organic solar cells, charge carrier collection is controlled by poor transport and very much affected by bimolecular recombination. In such cases, the FF is often limited by bimolecular recombination as explained by Neher and co-workers and others.[42–45] The recombination of two species has recently been characterized by Wilson et al. using numerical simulations of continuous-wave photoinduced absorption. This approach allows one to distinguish between direct recombination and trap-assisted recombination.[46] Moreover, the recombination losses during charge extraction have been quantified with a modified charge extraction technique developed by Wright et al.[47] In addition to the field dependence of the photocurrent arising from the competition between charge extraction and recombination, it is feasible that field-dependent photogeneration could also impose additional losses on the FF.

With these considerations in mind, the plots in Figure 4 show one minus the first-order (*G*) and second-order (*E*) losses derived from Figure 3, but as a function of voltage from −1.0 to 0.4 V, i.e., reverse bias to around the maximum power point voltage ($V_{mpp}$). The parameters *G* and *E* are convenient proxies for the generation and extraction efficiencies, respectively. In the figure, they are overlaid on the measured AM1.5G *J*–*V* curves (typical examples) for the optimized blend [50% PTB7 (a)], around the electron percolation threshold through the fullerene network [70% PTB7 (b)], and well below the threshold [90% PTB7 (c)]. From these plots, we can make the following

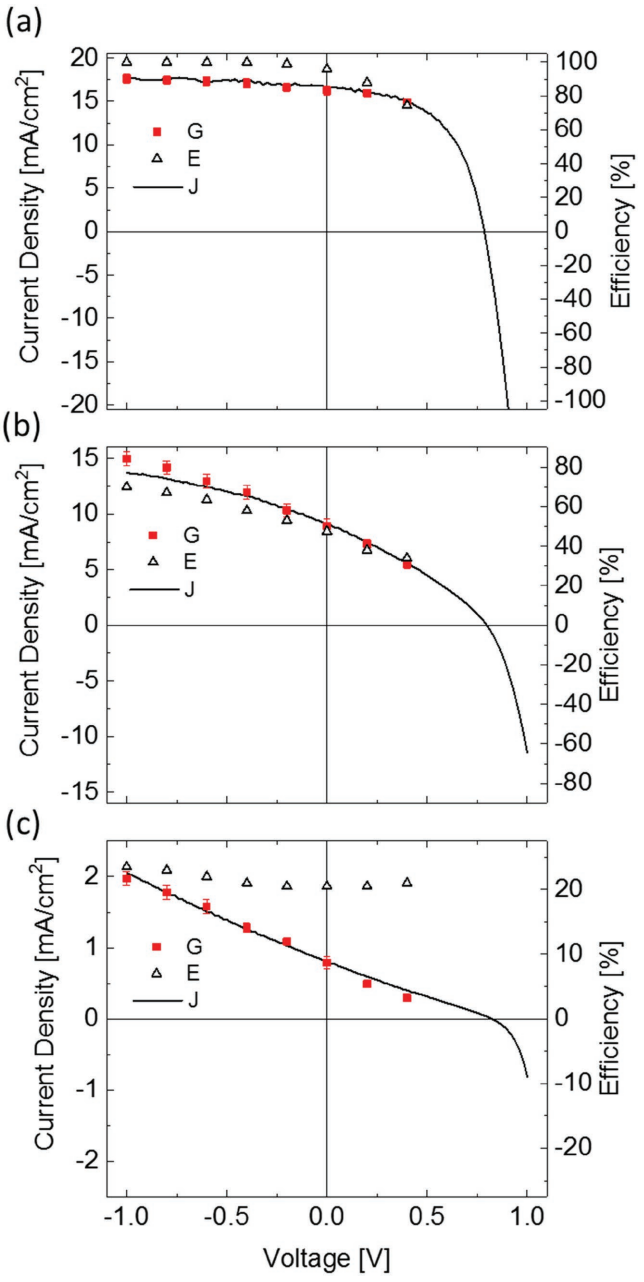


**Figure 4.** The parameters are plotted as $G = 1 -$ (first-order loss); and $E = 1 -$ (second-order loss), as proxies for generation (red, filled squares) and extraction (black, open triangles) efficiencies, respectively. a) 50%, b) 70%, and c) 90% PTB7 by weight versus applied bias (see Figure S5, Supporting Information for other devices).

observations: (i) First-order losses (and *G*) in the optimized blend (50 wt% PTB7) show only a very weak field dependence over the voltage range studied. However, second-order losses start to increase (and hence *E* decreases) moving toward forward bias. This is consistent with non-geminate losses being comparable to charge extraction as carrier densities approach the space charge limit near $V_{OC}$. This can be viewed as the standard, high efficiency BHJ case; (ii) in the 70 wt% PTB7 devices, both first- and second-order losses (and hence *G* and *E*) show

similar field dependencies in moving from reverse to forward bias. This behavior implies that the FF is limited by both field-dependent photogeneration and extraction—an unexpected behavior for a BHJ solar cell; and (iii) finally, in the 90 wt% PTB7 devices, the second-order losses (and hence $E$) are field invariant, but the first-order losses (and hence $G$) show a strong field dependence moving from reverse to forward bias. This indicates that the shape of the $J$–$V$ curve close to $V_{mpp}$ is dominated by geminate recombination (and related first-order losses). The observation is somewhat at odds with the general understanding that the FF in BHJs is limited by the competition between extraction and non-geminate recombination.[43] It suggests that the field dependence of the $J$–$V$ curve in "poor BHJ" blends with very imbalanced donor and acceptor concentrations is more akin to the field-assisted charge dissociation in organic semiconductor-based homojunction devices. This was originally proposed by Onsager, and then modified by Braun.[14,16]

## 4. Discussion

Overall, our results indicate that the IQE of BHJ organic solar cells is strongly correlated to the slower carrier mobility (Figure 1). This is in agreement with recently reported work showing that the charge generation yield is dependent upon the slower carrier mobility in BHJs rather than the sum of the mobilities as predicted by the Onsager–Braun model.[16,19] This fact is exemplified in **Figure 5**, which depicts the photogeneration efficiency (expressed as a percent charge generation yield from the IQE in the linear light intensity regime) as function of the slower carrier mobility determined from RPV. The implicit assumption is that the slower carrier is the electron since the plot refers to the fullerene subpercolation regime. The figure clearly shows a sharp rise in the charge generation yield as the electron mobility increases upon the formation of percolation pathways (i.e., the fullerene load increases around ≈70% PTB7 by weight; $\mu_e \approx 2 \times 10^{-5}$ cm$^2$ V$^{-1}$ s$^{-1}$). Likewise, there is

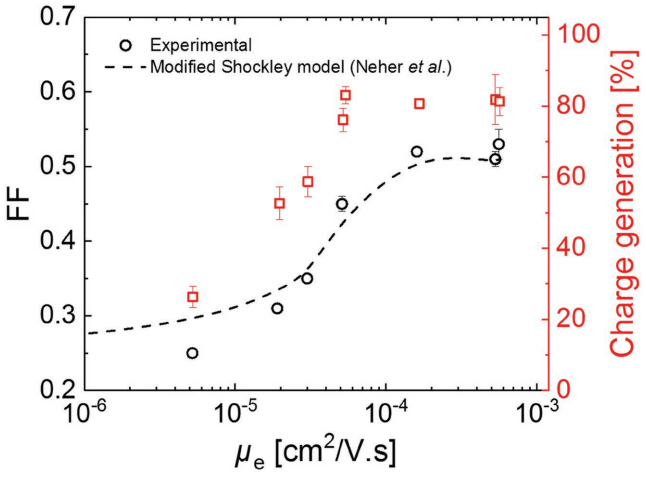


**Figure 5.** Charge generation efficiencies (from the IQE in the linear intensity regime), and experimentally measured FFs as a function of electron mobility, together with theoretically predicted values (black dashed line) based upon the modified Shockley equation in the citation.[11]

also a dramatic and concomitant improvement in the FF as the fullerene content approaches the optimal 1:1 ratio.

Figure 5 also compares the experimental FF and calculated FF (black dashed line) based upon a modified Shockley model as suggested by Neher et al.,[11] who incorporated imperfect charge collection into the conventional Shockley equation to explain the FF of BHJ organic solar cells. The proposed model reliably predicts the FF above the percolation threshold of the fullerene, where field-dependent first-order losses are negligible. The model is also applicable for the FF below the percolation threshold, when the generation rate in the model is appropriately considered field dependent as shown in Figure 4. Hence, we can conclude that in "poor BHJ" systems where extraction is inefficient (because of incomplete percolation pathways or very low carrier mobilities of one or both types), the FF is not only governed by the competition between charge extraction and bimolecular recombination, but also by the field dependence of the first-order losses and possibly charge generation. Ultimately, we should note that efficient BHJ organic solar cells exhibit field-independent charge generation as previously reported.[27] In either of these cases, the modified model of Neher et al. can be applied by considering field-dependent charge generation (or first-order losses).[11]

In conclusion, we have presented a comprehensive study of the recombination loss mechanisms in the model high efficiency BHJ organic solar cell system PTB7:$PC_{71}BM$ above and below the transport percolation limit of the fullerene acceptor. The first- and second-order losses are correlated with the slower carrier mobility, as is the IQE. With respect to electric-field dependence of the $J$–$V$ characteristics, we see distinct regimes: in efficient devices (i.e., the BHJ regime) above the fullerene percolation threshold, the FF is dominated by bimolecular recombination; significantly below the threshold, first-order (including photogeneration) losses are strongly field dependent; and in the intermediate regime, the FF is limited by both field-dependent photogeneration and extraction. The latter two regimes are somewhat atypical of BHJ systems, and in particular the low acceptor content devices are akin to field-assisted charge dissociation homojunctions as proposed by Onsager and Braun. Finally, we have shown that the efficient BHJ regime can be modeled using the recent modified Shockley approach.[11] This work clearly demonstrates the importance of accurate IQE analysis as a means to identify and quantify recombination losses in organic solar cells. It is an interesting question as to whether these findings in polymer:fullerene systems translate to emerging next high efficiency donor:acceptor BHJ combinations, and this is a subject of further work on our part.

## 5. Experimental Section

*Solar Cell Fabrication and Characterization*: Indium tin oxide-coated and prepatterned glass substrates (Xinyan: 15 Ω sq$^{-1}$) were first sonicated in Alconox solution (a detergent bath) at 80 °C for 10 min and then rubbed with a soft fabric, followed by sonication in deionized water, acetone, and 2-propanol for 10 min each, respectively. The substrates were then dried with nitrogen prior to spin coating the poly(3,4-ethylenedioxythiophene):poly(styrene sulfonate) (PEDOT:PSS) (Heraeus Clevios P VP AI 4083) layer. The thickness of the PEDOT:PSS layer spin coated for each cell at 5000 rpm for 30 s was measured as 30 ± 5 nm using a

Veeco Dektak 150 profilometer. The PEDOT:PSS-coated substrates were then annealed at 165 °C for 10 min under ambient conditions before transferring into a nitrogen atmosphere glove box ($O_2$ < 1 ppm, $H_2O$ < 1 ppm). $PC_{71}BM$ (American Dye Source) was dissolved in a solvent mixture consisting of 90% anhydrous CB and 10% anhydrous 1,2-dichlorobenzene (DCB) to prepare a 48 mg $mL^{-1}$ base solution. The $PC_{71}BM$ solution was stirred on a hot plate for stirring at 70 °C for 1 h and then filtered with a 0.2 μ PTFE filter after cooling down to room temperature. The filtered solution was added to each vial containing 6 mg of PTB7 step-by-step after being gradually diluted with the solvent mixture to obtain the desired polymer:fullerene solutions with different blend ratios ranging from 95% to 40% polymer content by weight. The polymer:fullerene solutions were further diluted so as to obtain 100 nm thick photoactive layers for each blend when spin coated at 600 rpm for 40 s. All the samples were annealed at 50 °C for 5 min in a glove box for additional solvent evaporation after active layer deposition. Then, the samples were loaded into the thermal evaporation chamber for metal electrode deposition. 1 nm Sm and 100 nm Al were sequentially evaporated on top of the organic films to form the cathode under a $10^{-6}$ mbar vacuum. A grid mask was used to achieve three devices on each substrate with a typical device area of 0.2 $cm^2$. *J–V* measurements were performed in a nitrogen atmosphere using a Keithley 2400 Source Measure Unit and Agilent B1500A semiconductor device analyzer. An Abet Sun 2000 Solar Simulator was used as a source of the simulated Air Mass 1.5 Global (AM1.5G) illumination. The light intensity output (≈1000 W $m^{-2}$) was calibrated with an NREL-certified silicon reference cell. The EQE spectra and the near normal incidence reflectance were characterized using a PV Measurements Inc. QEX7 system equipped with an NREL-certified photodiode. Integrated short-circuit EQE current densities and AM1.5G short-circuit current densities agreed to within 5%. For all measured solar cell parameters, five devices were averaged and standard deviations were calculated. Accurate IQEs were obtained from measured EQEs as previously described,[32] using transfer matrix simulations and the near normal incidence reflectance data.

*Light-IPC Measurements*: IPC measurements were conducted with a continuous wave 532 nm laser (Ningbo Lasever Inc.) with a power output of 1 W. Optically different density filters were used to attenuate the incident light intensity illuminating the device and the photogenerated current transients were recorded with an Agilent B1500A analyzer. Each data point acquired corresponded to a steady state photocurrent measurement of the given device at a certain laser power which was simultaneously recorded with a Si photodetector to normalize against noise.

*Mobility via RPV Measurements*: RPV transients for mobility measurement of both types of carriers were recorded with an oscilloscope (LeCroy WaveRunner 6200A) at different external load resistances ($R_{Load}$). A delay generator (Stanford Research Systems DG535) was used to trigger a function generator (Agilent 33250A) and a pulsed Nd:Yag laser (Brio Quantel) to photogenerate the carriers with a pulse length 5 ns/10 ns and a wavelength 532 nm. Optically density filters were used to attenuate the laser pulse intensity, so that the internal electric field of the device was not affected.

## Supporting Information

Supporting Information is available from the Wiley Online Library or from the author.

## Acknowledgements

A.Y. was supported by the University of Queensland International Postgraduate Research Scholarship. A.A. is a Sêr Cymru Rising Star Fellow. P.M. is a Sêr Cymru Research Chair, and was formally an Australian Research Council Discovery Outstanding Research Award Fellow. P.L.B. is an Australian Research Council Laureate Fellow (FL160100067).

## Conflict of Interest

The authors declare no conflict of interest.

## Keywords

bulk heterojunctions, charge transport, organic solar cells, percolation threshold, recombination losses

Received: November 27, 2017
Revised: January 30, 2018
Published online:

[1] K. Sun, Z. Xiao, S. Lu, W. Zajaczkowski, W. Pisula, E. Hanssen, J. M. White, R. M. Williamson, J. Subbiah, J. Ouyang, A. B. Holmes, W. W. H. Wong, D. J. Jones, *Nat. Commun.* **2015**, *6*, 6013.
[2] Z. C. He, B. Xiao, F. Liu, H. B. Wu, Y. L. Yang, S. Xiao, C. Wang, T. P. Russell, Y. Cao, *Nat. Photonics* **2015**, *9*, 174.
[3] Y. Jin, Z. Chen, S. Dong, N. Zheng, L. Ying, X. F. Jiang, F. Liu, F. Huang, Y. Cao, *Adv. Mater.* **2016**, *28*, 9811.
[4] W. Zhao, S. Li, H. Yao, S. Zhang, Y. Zhang, B. Yang, J. Hou, *J. Am. Chem. Soc.* **2017**, *139*, 7148.
[5] G. J. Hedley, A. J. Ward, A. Alekseev, C. T. Howells, E. R. Martins, L. A. Serrano, G. Cooke, A. Ruseckas, I. D. Samuel, *Nat. Commun.* **2013**, *4*, 2867.
[6] O. K. Kwon, M. A. Uddin, J.-H. Park, S. K. Park, T. L. Nguyen, H. Y. Woo, S. Y. Park, *Adv. Mater.* **2016**, *28*, 910.
[7] W. Shockley, H. J. Queisser, *J. Appl. Phys.* **1961**, *32*, 510.
[8] T. M. Clarke, J. R. Durrant, *Chem. Rev.* **2010**, *110*, 6736.
[9] C. Deibel, T. Strobel, V. Dyakonov, *Adv. Mater.* **2010**, *22*, 4097.
[10] A. Armin, I. Kassal, P. E. Shaw, M. Hambsch, M. Stolterfoht, D. M. Lyons, J. Li, Z. Shi, P. L. Burn, P. Meredith, *J. Am. Chem. Soc.* **2014**, *136*, 11465.
[11] D. Neher, J. Kniepert, A. Elimelech, L. J. Koster, *Sci. Rep.* **2016**, *6*, 24861.
[12] A. Armin, J. Subbiah, M. Stolterfoht, S. Shoaee, Z. Y. Xiao, S. R. Lu, D. J. Jones, P. Meredith, *Adv. Energy Mater.* **2016**, *6*, 1600939.
[13] M. Stolterfoht, B. Philippa, S. Shoaee, H. Jin, W. Jiang, R. D. White, P. L. Burn, P. Meredith, A. Pivrikas, *J. Phys. Chem. C* **2015**, *119*, 26866.
[14] L. Onsager, *Phys. Rev.* **1938**, *54*, 554.
[15] P. Langevin, *Ann. Chim. Phys.* **1903**, *28*, 122.
[16] C. L. Braun, *J. Chem. Phys.* **1984**, *80*, 4157.
[17] B. M. Savoie, A. Rao, A. A. Bakulin, S. Gelinas, B. Movaghar, R. H. Friend, T. J. Marks, M. A. Ratner, *J. Am. Chem. Soc.* **2014**, *136*, 2876.
[18] H. Utzat, S. D. Dimitrov, S. Wheeler, E. Collado-Fregoso, P. S. Tuladhar, B. C. Schroeder, I. McCulloch, J. R. Durrant, *J. Phys. Chem. C* **2017**, *121*, 9790.
[19] M. Stolterfoht, A. Armin, S. Shoaee, I. Kassal, P. Burn, P. Meredith, *Nat. Commun.* **2016**, *7*, 11944.
[20] P. W. M. Blom, M. J. M. de Jong, J. J. M. Vleggaar, *Appl. Phys. Lett.* **1996**, *68*, 3308.
[21] L. J. A. Koster, V. D. Mihailetchi, P. W. M. Blom, *Appl. Phys. Lett.* **2006**, *88*, 052104.
[22] J. C. Blakesley, H. S. Clubb, N. C. Greenham, *Phys. Rev. B* **2010**, *81*, 045210.
[23] J. Kniepert, M. Schubert, J. C. Blakesley, D. Neher, *J. Phys. Chem. Lett.* **2011**, *2*, 700.
[24] V. Coropceanu, J.-L. Brédas, S. Mehraeen, *J. Phys. Chem. C* **2017**, *121*, 24954.

[25] S. Shoaee, T. M. Clarke, C. Huang, S. Barlow, S. R. Marder, M. Heeney, I. McCulloch, J. R. Durrant, *J. Am. Chem. Soc.* **2010**, *132*, 12919.
[26] S. N. Hood, I. Kassal, *J. Phys. Chem. Lett.* **2016**, *7*, 4495.
[27] M. Stolterfoht, S. Shoaee, A. Armin, H. Jin, I. Kassal, W. Jiang, P. Burn, P. Meredith, *Adv. Energy Mater.* **2017**, *7*, 1601379.
[28] A. Foertig, J. Kniepert, M. Gluecker, T. Brenner, V. Dyakonov, D. Neher, C. Deibel, *Adv. Funct. Mater.* **2014**, *24*, 1306.
[29] J. Kniepert, I. Lange, J. Heidbrink, J. Kurpiers, T. J. K. Brenner, L. J. A. Koster, D. Neher, *J. Phys. Chem. C* **2015**, *119*, 8310.
[30] B. Philippa, M. Stolterfoht, P. L. Burn, G. Juska, P. Meredith, R. D. White, A. Pivrikas, *Sci. Rep.* **2014**, *4*, 5695.
[31] M. Stolterfoht, A. Armin, B. Philippa, R. D. White, P. L. Burn, P. Meredith, G. Juska, A. Pivrikas, *Sci. Rep.* **2015**, *5*, 9949.
[32] A. Armin, M. Velusamy, P. Wolfer, Y. L. Zhang, P. L. Burn, P. Meredith, A. Pivrikas, *ACS Photonics* **2014**, *1*, 173.
[33] Z. He, C. Zhong, S. Su, M. Xu, H. Wu, Y. Cao, *Nat. Photonics* **2012**, *6*, 591.
[34] Y. Liang, Z. Xu, J. Xia, S.-T. Tsai, Y. Wu, G. Li, C. Ray, L. Yu, *Adv. Mater.* **2010**, *22*, E135.
[35] F. Liu, W. Zhao, J. R. Tumbleston, C. Wang, Y. Gu, D. Wang, A. L. Briseno, H. Ade, T. P. Russell, *Adv. Energy Mater.* **2014**, *4*, 1301377.
[36] Z. Li, G. Lakhwani, N. C. Greenham, C. R. McNeill, *J. Appl. Phys.* **2013**, *114*, 034502.
[37] L. J. A. Koster, M. Kemerink, M. M. Wienk, K. Maturová, R. A. J. Janssen, *Adv. Mater.* **2011**, *23*, 1670.
[38] M. Lenes, M. Morana, C. J. Brabec, P. W. M. Blom, *Adv. Funct. Mater.* **2009**, *19*, 1106.
[39] A. Armin, M. Hambsch, I. K. Kim, P. L. Burn, P. Meredith, E. B. Namdas, *Laser Photonics Rev.* **2014**, *8*, 924.
[40] V. D. Mihailetchi, J. Wildeman, P. W. M. Blom, *Phys. Rev. Lett.* **2005**, *94*, 126602.
[41] A. M. Goodman, A. Rose, *J. Appl. Phys.* **1971**, *42*, 2823.
[42] M. Stolterfoht, A. Armin, B. Philippa, D. Neher, *J. Phys. Chem. Lett.* **2016**, *7*, 4716.
[43] D. Bartesaghi, C. Perez Idel, J. Kniepert, S. Roland, M. Turbiez, D. Neher, L. J. Koster, *Nat. Commun.* **2015**, *6*, 7083.
[44] A. Armin, Z. Chen, Y. Jin, K. Zhang, F. Huang, S. Shoaee, *Adv. Energy Mater.* **2017**, 1701450, https://doi.org/10.1002/aenm.201701450.
[45] G. Zhang, T. M. Clarke, A. J. Mozer, *J. Phys. Chem. C* **2016**, *120*, 7033.
[46] N. M. Wilson, S. Sandén, O. J. Sandberg, R. Österbacka, *J. Appl. Phys.* **2017**, *121*, 095701.
[47] B. Wright, Y. Nakajima, T. M. Clarke, K. Okuda, H. Paananen, A. J. Mozer, S. Mori, *Adv. Energy Mater.* **2017**, *7*, 1602026.